電気学会論文誌●（●●●●●●●部門誌）
IEEJ Transactions on ●●●●●●●●●●●●●●●●
Vol.●● No.● pp.●-●● DOI: ●.●●/ieejeiss.●●.●

Paper

Coil Design Method Considering Power, Efficiency and Magnetic Field Strength of Coreless Coils Using Numerical Analysis in Wireless Power Transfer

Yuto Yamada*a) Student Member, Soma Hasegawa* Student Member
Takehiro Imura* Member, Yoichi Hori* Fellow

(Manuscript received Jan. 00, 20XX, revised May 00, 20XX)

Wireless power transfer to electric vehicles while driving is a technology that is currently attracting attention as it has the potential to solve the problems faced by EVs that will become popular worldwide in the future. In the case of Dynamic Wireless Power Transfer (DWPT) to electric vehicles, it is necessary to transmit the required power with high efficiency and ensure safety. While there are multiple safety requirements, there are also regulatory values for the magnetic field strength emitted from the coil, which must be satisfied before it can be implemented in society. This research aims to speed up the design of coils by using only numerical analysis, in contrast to conventional coil design using electromagnetic field analysis. In the future construction of wireless power transfer systems, it is of great significance to discuss the design using only numerical analysis, as there are many design parameters. Experiments were carried out and compared with the numerical analysis and found to be in agreement. A power transmission of 20 kW converted value was carried out to verify the effect of the size, pitch and number of turns of the transmission coils on the efficiency and magnetic field strength. The effect of input voltage was also discussed by simulation, and the optimum coil was derived. As a result, when the coil size was 800 × 600 mm, the number of turns was 46, the pitch was 6.1 mm and the input voltage was 1400 V, the analysis showed that a power transmission of 20 kW with an efficiency of 99.3% and a far magnetic field leakage strength of 81.6 dBμA/m could be achieved. Even with a coreless coil, the magnetic field strength could be below the regulation value.

Keywords : Dynamic Wireless Power Transfer, Coil Design, Far-Magnetic Field, Near-Magnetic Field, Inductive Wireless Power Transmission

1. Introduction

Wireless power transfer using magnetic field resonance can transmit power at high efficiency and high power, and is widely used in various devices from the point of view of its convenience. Due to the global decarbonization trend, vehicles are beginning to shift from conventional Internal Combustion Engine Vehicles (ICEV) to battery-powered and motor-driven electric vehicles. The challenges facing Battery powered Electric Vehicles (BEVs) today include the need for high weight batteries to ensure cruising range, the associated increase in vehicle price, and the lower cost of electricity due to the increased vehicle weight, the lack of power transmission facilities and the time required for power charging, accidents involving cables during power supply, and cruising range reduction due to heating and cooling and battery depletion in cold climates [1] [2] [3] [4]. In addition, as BEVs continue to expand in the future, issues such as harmful substances generated during battery production, disposal problems of degraded batteries, and further rising costs and shortages of rare metals used during production and insufficient power generation capacity [5] [6] [7] can be considered. Dynamic Wireless Power Transfer (DWPT) is a system in which power is supplied wirelessly while driving by installing a power transmission coil on the infrastructure side and a power receiving coil on the vehicle side. As the power is supplied while the vehicle is running, the system enables an extended cruising range with a small battery capacity, and is also expected to extend battery life due to the repetition of small charge and discharge cycles [8] [9]. The global share of electric vehicles is currently 12% and is expected to increase in the future due to the global trend towards banning the launch of new internal combustion engine vehicle [10]. Therefore, dynamic wireless power transfer to electric vehicles has been actively researched in recent years as a way to solve the current challenges faced by battery EVs and the new challenges that will arise when the share of battery EVs expands [11] [12]. Among these, research on coil optimization has become a very important topic as it directly influences the DWPT system, and in much of the literature, optimization using electromagnetic field analysis is the dominant method. Electromagnetic field analysis is already well established and can simulate complex peripheral environments, but it has issues such as the need for a large analysis PC (Personal Computer) and the analysis time required [13]. Considering the design of the entire wireless power transfer system as well as the coils, the number of design parameters is very large and the verification patterns are enormous, requiring faster analysis such as numerical analysis. In addition, it is significant that the design is carried out only by numerical analysis, which leads to a theoretical explanation of each parameter [14] .

a) Correspondence to: Yuto Yamada.
Email:yuto.yamada20@gmail.com
* Tokyo University of Science, Factory and Engineering, Imura-Hori Laboratory, Building12, Noda, Chiba, Japan.

In [15], the economic viability of social implementation of DWPT is examined, and a return on investment is possible for society as a whole. It has also been shown that it is more economical to invest more in the power supply equipment, i.e. to increase the power transmission capacity [9] [16] , and higher power is also a major challenge in wireless power transfer. In order to implement dynamic wireless power transfer to electric vehicles in society, it is necessary to ensure the required power transfer characteristics at low cost and with a guarantee of safety. One of the most frequently discussed safety issues is magnetic field leakage [17] and from the viewpoint of damage from human exposure to time varying electromagnetic fields (EMFs), the ICNIRP (International Commission on Non-Ionizing Radiation Protection) has set a limit of 27 μT [18] [19] for the magnetic field strength at a point 20 cm from the vehicle body. In addition, for the purpose of preventing electromagnetic interference with precision equipment (Electromagnetic Compatibility: EMC), a regulation value of 67.8 dBμA/m for magnetic field strength in an area more than 10 m away from the vehicle body has been established [18] [20]. However, in the frequency range planned for use in wireless power transfer to electric vehicles, a further relaxed regulation value, 82.8 dBμA/m, has been set [18]. The 82.8 dBμA/m is adopted in this study because the first introduction of dynamic wireless power transfer is envisaged for environments such as highways where people are not allowed to enter the surrounding area.

Although some studies have introduced cancellation coils or complex shielding materials to suppress magnetic fields leakage [21] [22] [23], nothing is as simple and inexpensive as suppressing magnetic fields leakage generated by a coil. [24] studied only far-magnetic field strength in a simulation. While static wireless power transfer to electric vehicles has been standardized in SAE J2954 for 2020 [18], dynamic wireless power transfer has not yet been defined, and this research is important from the point of view that it is essential to construct an optimal system at an early stage.

In this study, a coil with high power transmission efficiency and the lowest magnetic field leakage under 20 kW power transmission is considered. Both far and near magnetic field leakage were considered experimentally and compared with theory. The design parameters used were the size of the transmission coil, the number of turns of the transmission coil, the pitch of the transmission coil, and the input voltage and confirmed that some coils were below the regulated value of the magnetic field strength.

The circuit characteristics of the S-S circuit and the derivation of the internal resistance R_i $(i = 1,2)$ and mutual inductance L_m of the coils are presented in Chapter 2, the derivation of the magnetic field strength at an arbitrary point P using vector potentials is explained in Chapter 3 and the results of numerical analysis are compared with experimental results in Chapter 4. The influence of each design parameter on the magnetic field strength is discussed in Chapter 5, and conclusions are presented in Chapter 6. The accuracy of the derivation of the neighborhood electromagnetic field is presented in the Appendix.

2. Coil Design Method for SS Circuit

This section presents the circuit equations for wireless power transfer using the SS (Series-Series) method, which is the simplest method for wireless power transfer to electric vehicles, in which an inductor and a capacitor are connected in series and both the primary and secondary sides are resonant, and explains how the internal resistance R_i of the coil, the derivation of the self-inductance L_i, and the derivation of the mutual inductance L_m [24] [25] [26].

2.1 Derivation of circuit characteristics of SS circuits

Consider the SS circuit and equivalent circuit as shown in Fig 1. A full-wave rectifier is sandwiched between the loads.

The input voltage is represented by V_1, the resonant capacitor by C_i $(i = 1,2)$, the inductance by L_i $(i = 1,2)$, the mutual inductance by L_m, the internal resistance by R_i $(i = 1,2)$ and the load by $R_L{}'$. The load from the AC side is R_L. (1) shows the resonance conditions of the circuit.

$$\omega_0 = 2\pi f = \frac{1}{\sqrt{L_1 C_1}} = \frac{1}{\sqrt{L_2 C_2}} \tag{1}$$

From the circuit equations, the currents I_1 and I_2 can be expressed as (2) and (3), showing that the phase differs by π/2 between the primary and secondary sides [26].

$$I_1 = \frac{R_2 + R_L}{R_1(R_2 + R_L) + (\omega_0 L_m)^2} V_1 \tag{2}$$

$$I_2 = j\frac{\omega_0 L_m}{R_1(R_2 + R_L) + (\omega_0 L_m)^2} V_1 \tag{3}$$

The power P_2 consumed by the resistance load R_L and the power transmission efficiency η can be expressed by (4) and (5), respectively. Power P_2 represents the AC power received.

$$P_2 = \frac{R_L(\omega_0 L_m)^2}{\{R_1(R_2 + R_L) + (\omega_0 L_m)^2\}^2} V_1^2 \tag{4}$$

$$\eta = \frac{R_L(\omega_0 L_m)^2}{(R_2 + R_L)\{R_1(R_2 + R_L) + (\omega_0 L_m)^2\}} \tag{5}$$

When a rectifier is sandwiched, the relationship between the load R_L from the AC side and the load $R_L{}'$ from the DC side can be expressed by (6) [25].

$$R_L{}' = \frac{\pi^2}{8} R_L \tag{6}$$

2.2 Derivation of the internal resistance *R* of the coil

Wireless power transfer to EVs uses AC power in the 85 kHz band, and to reduce AC resistance, a Litz wire with a bunch of thin strands is used. AC power losses include copper loss, iron loss, and radiation loss, but this study focuses on copper loss and derives the coil resistance because the study is conducted using a core-less coil and the coil is small compared to the wavelength. The copper loss of Litz wire can be mainly divided into skin effect loss and proximity effect loss, which can be considered independently. The skin effect loss $P_{S,Litz}$ [W/m], and proximity effect loss $P_{P,Litz}$ [W/m] are shown in (7) and (8), respectively.

The number of strands of Litz wire is *n*, the strand diameter is d_i, and the parameters necessary for resistance calculation, such as skin depth δ, DC resistance R_{DC}, and RMS current per strand I_{rms}, are summarized in Table 1. (8) consists of the external magnetic field H_e and the internal magnetic field H_i of the Litz wire, where H_e can be expressed by (11) and H_i is derived by the PEEC method [27]. Pitch p, the distance between Litz wires, is shown in Fig 2.

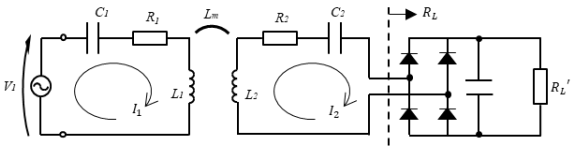

Fig 1 Equivalent circuit in magnetic field resonance coupling of (S-S).

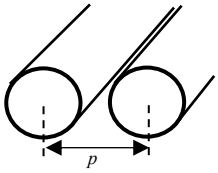

Fig 2 Pitch (Distance between wire to wire)

Table 1 Parameters required for resistance calculation.

δ	R_{DC}	ξ	I_{rms}
$\frac{1}{\sqrt{\pi\mu_0\sigma f}}$	$\frac{4}{\sigma\pi d_i^2}$	$\frac{d_i}{\sqrt{2}\delta}$	$\frac{\hat{I}}{\sqrt{2}n}$

$$P_{S,Litz} = n \cdot F_R(f) \cdot R_{DC} \cdot I_{rms}^2 \tag{7}$$

$$P_{P,Litz} = n \cdot G_R(f) \cdot R_{DC} \cdot \left(H_e^2 + H_i^2\right) \tag{8}$$

$$F_R = \frac{\xi}{2\sqrt{2}} \cdot \frac{1}{\mathrm{ber}_1(\xi)^2 + \mathrm{bei}_1(\xi)^2} \cdot \{-\mathrm{ber}_0(\xi)\mathrm{ber}_1(\xi) + \mathrm{ber}_0(\xi)\mathrm{bei}_1(\xi) - \mathrm{bei}_0(\xi)\mathrm{ber}_1(\xi) - \mathrm{bei}_0(\xi)\mathrm{bei}_1(\xi)\} \tag{9}$$

$$G_R = -\frac{\xi\pi^2 d_i^2}{2\sqrt{2}} \cdot \frac{1}{\mathrm{ber}_0(\xi)^2 + \mathrm{bei}_0(\xi)^2} \cdot \{\mathrm{ber}_2(\xi)\mathrm{ber}_1(\xi) + \mathrm{ber}_2(\xi)\mathrm{bei}_1(\xi) - \mathrm{bei}_2(\xi)\mathrm{ber}_1(\xi) + \mathrm{bei}_2(\xi)\mathrm{bei}_1(\xi)\} \tag{10}$$

$$H_e = \frac{\hat{I}}{2\pi p} \tag{11}$$

From the above, the resistance per unit length of Litz wire is obtained, and this is the internal resistance R_i (i=1,2) of the coil.

2.3 Derivation of the self-inductance L of the coil

From (1)-(5), it can be seen that the derivation of the circuit the coils and the mutual inductance L_m. However, for actual power transmission, it is also essential to derive the self-inductance and the associated resonant capacitor. (12) is the formula for the derivation of the self-inductance of a square spiral coil [28], where d_a is the diameter of the Litz wire conductor and α is the length of the gap between the Litz wires, expressed as $\alpha = p - d_a$. The parameters used to derive the self-inductance are shown in Fig 3.

$$L = 0.635\mu d_{ave} N^2 \left\{\ln\left(\frac{2.07}{\rho}\right) + 0.18\rho + 0.13\rho^2\right\} \tag{12}$$

$$d_{ave} = \frac{1}{4}(X_{in} + X_{out} + Y_{in} + Y_{out}) \tag{13}$$

$$\rho = \frac{1}{2}\left(\frac{X_{out} - X_{in}}{X_{out} + X_{in}} + \frac{Y_{out} - Y_{in}}{Y_{out} + Y_{in}}\right) \tag{14}$$

2.4 Derivation of the mutual inductance L_m of the coil

During wireless power transfer, coupling occurs between the transmitting and receiving coils, the proportion of which is

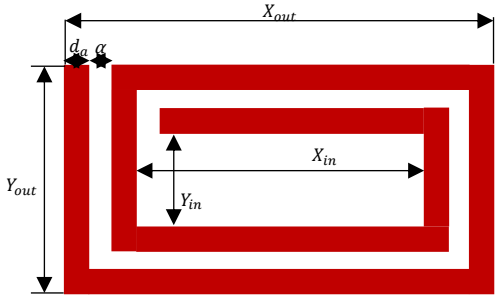

Fig 3 Coil parameters used to derive self-inductance.

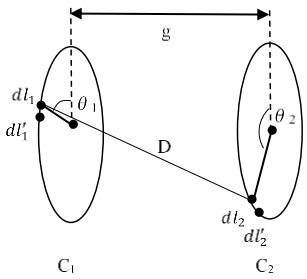

Fig 4 Parameters of the Neumann equation

expressed by the coupling coefficient k. Together with the coupling coefficient and the self-inductance, the mutual inductance can be obtained, which is a very important parameter in circuit calculations. The equation that can directly express the mutual inductance is called the Neumann equation and can be expressed as (15). The parameters used in (15) are shown in Fig 4.

$$L_m = \frac{\mu_0}{4\pi}\oint_{C1}\oint_{C2}\frac{dl_1 dl_2}{D} \tag{15}$$

3. Derivation of magnetic field strength using vector potentials

In wireless power transfer using magnetic field resonance, a magnetic field is generated from the coil. During power transmission, the magnetic field spreads around the coil and has a negative impact on surrounding humans and precision equipment, for which regulation values have been established in SAE J2954, CISPR, and ICNIRP. In this chapter, the magnetic field strength was derived by vector potential using the current value flowing in the coil [29]. Compared to the derivation of magnetic field strength using Biot-Savart, the use of approximations makes it possible to derive the magnetic field strength with a concise function of the number of turns, which makes it easier to design coils.

The vector potential at a distance r generated by the current I flowing in the microline $\Delta\boldsymbol{s}$ is expressed by (16).

$$\Delta\boldsymbol{A} = \frac{\mu_0 I}{4\pi r}\Delta\boldsymbol{s} \tag{16}$$

Considering a rectangular current loop as in Fig 5, the vector potential $\boldsymbol{A}$ at point P(x,y,z) has only A_x and A_y components, as in (17) and (18), respectively.

$$A_x \approx \frac{\mu_0 aI}{4\pi}\left(\frac{1}{r_4} - \frac{1}{r_2}\right) \tag{17}$$

$$A_y \approx \frac{\mu_0 bI}{4\pi}\left(\frac{1}{r_1} - \frac{1}{r_3}\right) \tag{18}$$

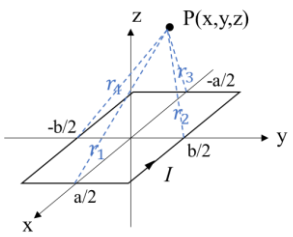

Fig 5 Parameters used for magnetic field calculation from vector potential.

Assuming $a, b \ll r$, the vector potential can be expressed as (19). However, $r = \sqrt{x^2 + y^2 + z^2}$ thereafter.

$$\boldsymbol{A}(\boldsymbol{r}) \approx \left(-\frac{\mu_0 abI}{4\pi}\frac{y}{r^3}, \frac{\mu_0 abI}{4\pi}\frac{x}{r^3}, 0 \right) \tag{19}$$

Calculate the magnetic field using the vector potential at point P. From $\boldsymbol{B} \equiv rot\, \boldsymbol{A}$, $\boldsymbol{B} = \mu_0 \boldsymbol{H}$ the magnetic field at point P is obtained as (20)-(22).

$$H_x = \frac{abI}{4\pi}\frac{3xz}{r^5} \tag{20}$$

$$H_y = \frac{abI}{4\pi}\frac{3yz}{r^5} \tag{21}$$

$$H_z = \frac{abI}{4\pi}\frac{2z^2 - x^2 - y^2}{r^5} \tag{22}$$

Assuming a coil with *n* turns as *n* loops as shown in Fig 6, ab in the above equation represents the sum of the area of each loop. Therefore, it can be expressed as in (23).

$$ab = \sum_{k=1}^{n} a_k b_k \tag{23}$$

$$a_k = a_1 - 2p(n-1) \tag{24}$$

$$b_k = b_1 - 2p(n-1) \tag{25}$$

Next, the magnetic field $\boldsymbol{H_p}$ at point P is obtained for the case where there are two coils, one primary and one secondary, as shown in Fig 7. $\boldsymbol{H_p}$ is calculated by finding and combining the magnetic field $\boldsymbol{H_{Tx}}$ due to the primary coil and the magnetic field $\boldsymbol{H_{Rx}}$ due to the secondary coil, respectively.

When the phase difference θ between the primary and secondary currents is considered, the magnetic fields generated by the primary and secondary coils can be expressed as (26) and (27). However,

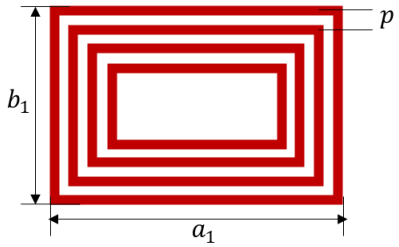

Fig 6 Coil shape used for magnetic field calculation.

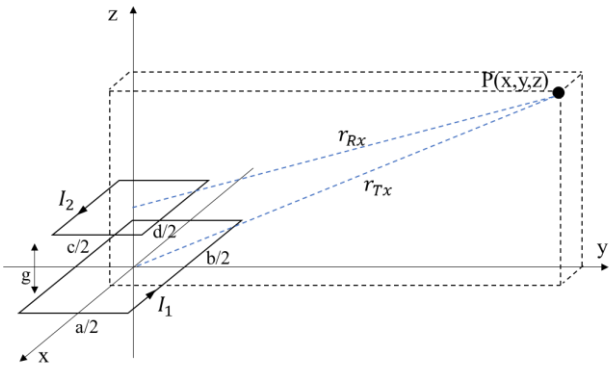

Fig 7 Parameters used for magnetic field calculation from vector potential with both primary and secondary coil.

$\sum_{k=1}^{n} a_k b_k$, $\sum_{k=1}^{m} c_k d_k$ are the sum of the loop areas of the primary and secondary coils, respectively, approximating $a_k, b_k \ll r_{Tx}$, $c_k, d_k \ll r_{Rx}$.

$$\boldsymbol{H_{Tx}} = \begin{pmatrix} \frac{\sum_{k=1}^{n} a_k b_k}{4\pi}\frac{3xz}{{r_{Tx}}^5} \cdot I_1 \sin\omega t \\ \frac{\sum_{k=1}^{n} a_k b_k}{4\pi}\frac{3yz}{{r_{Tx}}^5} \cdot I_1 \sin\omega t \\ \frac{\sum_{k=1}^{n} a_k b_k}{4\pi}\frac{2z^2 - x^2 - y^2}{{r_{Tx}}^5} \cdot I_1 \sin\omega t \end{pmatrix} \tag{26}$$

$$\boldsymbol{H_{Rx}} = \begin{pmatrix} \frac{\sum_{k=1}^{m} c_k d_k}{4\pi}\frac{3x(z-g)}{{r_{Rx}}^5} \cdot I_2 \sin(\omega t + \theta) \\ \frac{\sum_{k=1}^{m} c_k d_k}{4\pi}\frac{3y(z-g)}{{r_{Rx}}^5} \cdot I_2 \sin(\omega t + \theta) \\ \frac{\sum_{k=1}^{m} c_k d_k}{4\pi}\frac{2(z-g)^2 - x^2 - y^2}{{r_{Rx}}^5} \cdot I_2 \sin(\omega t + \theta) \end{pmatrix} \tag{27}$$

$$\left|\boldsymbol{H_p}\right| = \left|\boldsymbol{H_{Tx}} + \boldsymbol{H_{Rx}}\right| \tag{28}$$

From (26)-(27), the magnetic field at any point could be derived. Note that if the measurement point is close to the coil loop, the error may be larger. Derivation accuracy is discussed in the Appendix.

4. Comparison of theory and experimental validation.

In this section, a comparison of the contents of Chapters 2 and 3 with actual measurements is made. 4.1 compares the characteristics of the coils actually produced, and 4.2 compares the generated magnetic field and other circuit characteristics during the actual power transmission experiment. The purpose of this chapter is to ensure that the theory agrees with the measurements.

4.1 Comparison of the accuracy of deriving the internal resistance and self-inductance of a coil

Several types of coils were produced, including coils with a uniform number of turns and pitch but different coil sizes, coils with a uniform coil size and the number of turns but a different pitch, and coils with a uniform coil size and pitch but a different number of turns. The internal resistance and self-inductance of the coil were compared with measured values using the theory presented in Chapter 2. Fig 8 shows the produced power transmission coil. The Litz wire used has a strand diameter of 0.05 mm and a number of strands of 4,000. The length of the transmission coil in the y-direction was fixed at 600 mm. (a) shows the number of coil turns fixed at 6 with a pitch of 9.1 mm and the length in the x-direction varied from 800 mm, 1100 mm, 1400 mm, 1700 mm and 2000 mm. (b) shows the number of turns with 6 turns and the length in the x-direction fixed at 1700 mm, with the pitch varied from 5.1 mm, 9.1 mm, 18.1 mm and 27.1 mm. (c) shows the number of turns varied from 6, 11, 16, 21 and 26 coils when the length in the x-direction is fixed at 1700 mm and the pitch at 9.1 mm.

Fig 9-Fig 11 shows a comparison of experimental and calculated values of self-inductance and internal resistance for each of the patterns (a)-(c) in Fig 8 according to the method from [28] [26] [27]. For inductance, the error increases to around 10% when the pitch is increased, but the other coils with a pitch of 9.1 mm show very good agreement. The cause of the increase in error due to the wider pitch is that the coils produced this time use only Litz wire to maintain the wire-to-wire contact, which is thought to increase distortion.

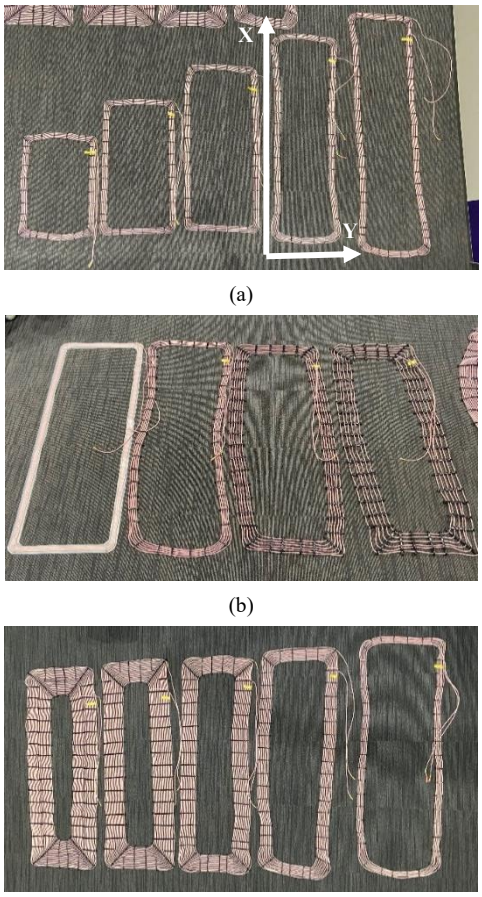

(a)

(b)

(c)

Fig 8 Coils used in the experiment. (a) Change in coil size (b) Change in coil pitch (c) Change in number of coil turns. (The long sides are in the x-direction (direction of vehicle travel) and the short sides are in the y-direction (direction of vehicle width)).

In addition, the formula is given in (12) uses the average of the long and short sides, which is more accurate when close to a square, so the inner turns may depart from the square more as the pitch increases. Errors are also found for the internal resistance, but the trend is very well captured and fast numerical analysis is found to be possible. The reason for the larger measured values than in the numerical analysis may be that the influence of the resistance component at the terminals was not taken into account, or that only the proximity effect from neighboring wires was taken into account for simplicity. This can be read from the fact that the error spreads as the number of turns increases. However, it was found that both self-inductance and internal resistance can be derived only by numerical analysis.

4.2 Comparison of experimental and analytical values from power transmission.

Here, a power transmission of 30 W was carried out and the experimental results were compared with the values derived by theory. The transmission distance was 220 mm and the power receiving coil had a coil size of 800 × 600 mm, with 7 turns and a pitch of 11 mm. The Litz wire used in the power receiving coil was a strand diameter of 0.05 mm and the number of strands was 10,000. Fig 12 shows the coil sizes used in the experiments. The circuit uses the same SS circuit as in Fig 1, and the efficiency is AC to AC efficiency using the power before the rectifier.

For the power transmission coils, a length of 1700 mm is shown as an example, but the length in the x-direction was changed for the experiments and discussion. Fig 13 and Fig 14 show a scene from the experiment. The measurement points for the near magnetic field leakage were 1.1 m in the y-direction and 1 m in the z-direction, as it was assumed that a point at a height of 1 m was to be measured 0.2 m from the vehicle body, which was 3800 mm wide.

For the far magnetic field leakage, the magnetic field strength was measured at 11.9 m in the y-direction and 1 m in the z-direction, as the measurement was made using a turntable at 11.9 m centered on the coil used for power transmission. A sinusoidal voltage at 85kHz was applied with a Bipolar Power Supply (KIKUSUI: PBZ40-10) and power was obtained using a rectifier and electronic load (TAKASAGO: FK-3-200-L) on the secondary side. Current,

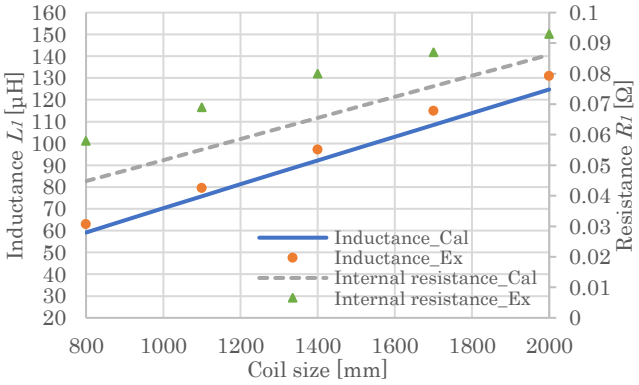

Fig 9 Comparison of experimental and theoretical values of inductance and internal resistance for each coil size (x direction).

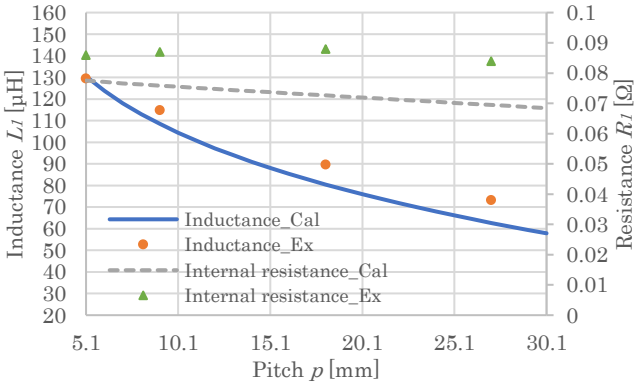

Fig 10 Comparison of experimental and theoretical values of inductance and internal resistance for each pitch.

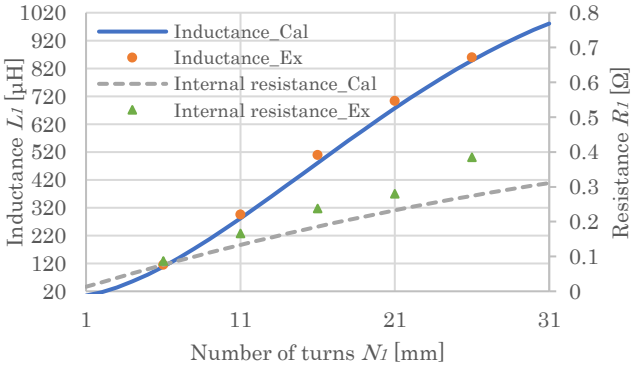

Fig 11 Comparison of experimental and theoretical values of inductance and internal resistance for each number of turns.

voltage and power were measured with an oscilloscope (TELEDYNE: 6034A), the near magnetic field was measured with a MAGNETIC FIELD HiTESTER (HIOKI: FT3470-51) and the far magnetic field with a Loop Antenna (ETS-LINDGREN: Model 6502). The voltage and power received were set to uniform conditions using each of the transmission coils produced in Chapter 4. The power received was adjusted by the load. The experimental data shown below is the conversion of a 30 W power transmission at an input voltage of approximately 23 Vrms into a 20 kW power transmission at a 600 Vrms input. From (4), the power is proportional to the square of the input voltage, and from (2) and (3), the current value is proportional to the input voltage. From (26) and (27), the magnetic field strength is proportional to the current value, which can be converted. The power received is assumed to be the AC side power. Efficiency is also calculated by AC to AC.

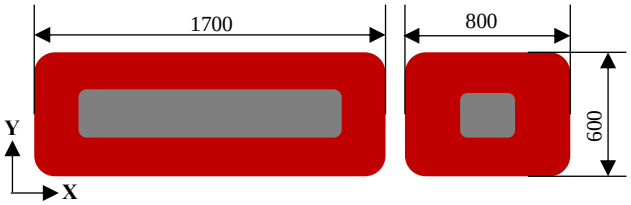

Fig 12 Coil size of transmission coil (Tx) and receiving coil (Rx).

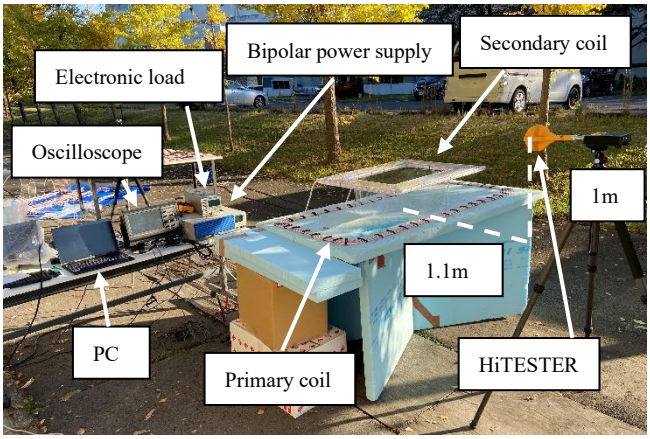

Fig 13 Scenes from power transmission experiments and measurements of nearby magnetic fields.

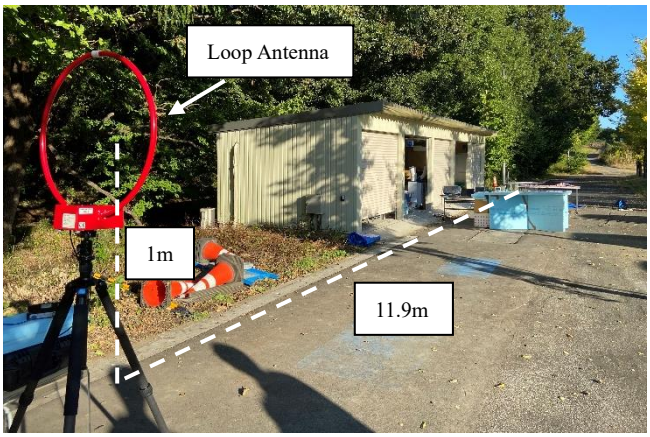

Fig 14 Scene of measurement of the far magnetic field leakage.

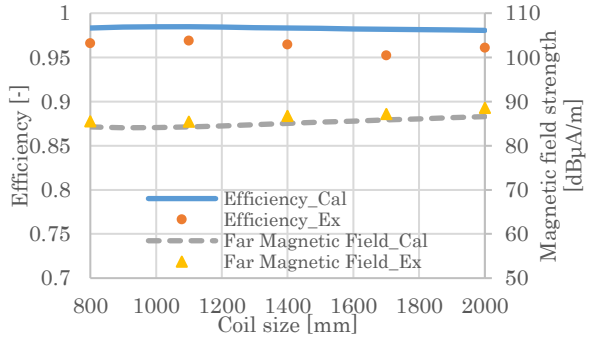

(a)

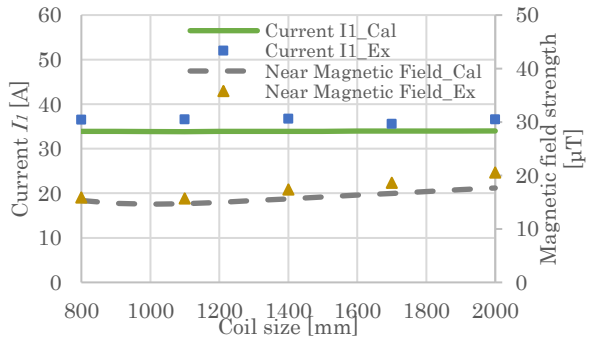

(b)

Fig 15 Comparison of experimental and calculated values of efficiency and far and near magnetic field strength and primary current for various coil sizes. (a) Efficiency and far magnetic field strength. (b) Primary current and near magnetic field strength.

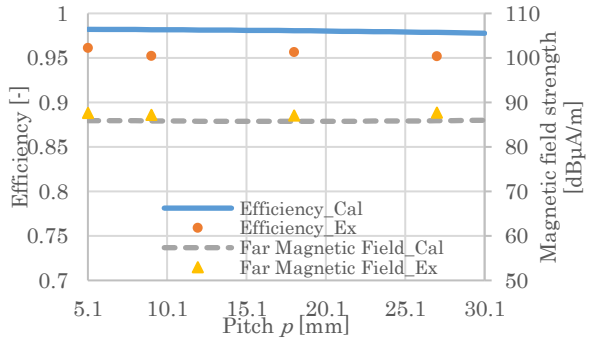

(a)

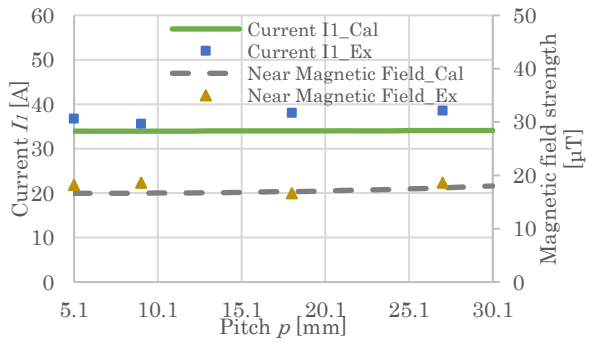

(b)

Fig 16 Comparison of experimental and calculated values of efficiency and far and near magnetic field strength and primary current for various pitch. (a) Efficiency and far magnetic field strength. (b) Primary current and near magnetic field strength.

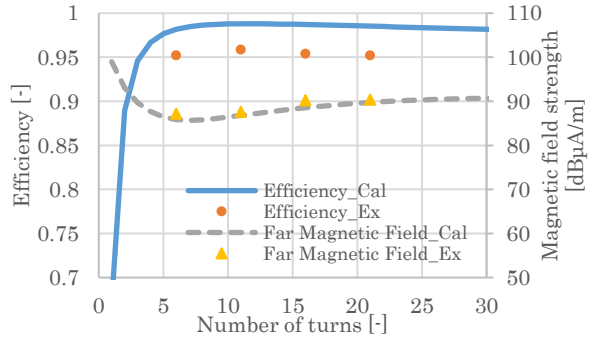

(a)

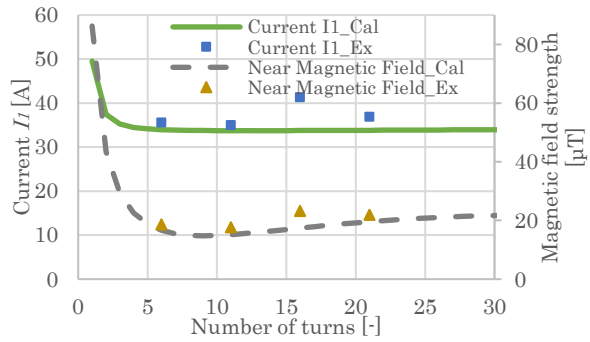

(b)

Fig 17 Comparison of experimental and calculated values of efficiency and far and near magnetic field strength and primary current for various number of turns. (a) Efficiency and far magnetic field strength. (b) Primary current and near magnetic field strength.

Fig 15-Fig 17 show that the experimented and calculated values are in good agreement. The main causes of the error are considered to be that the internal resistance of the capacitor is not taken into account in the calculation, the resonance misalignment between the coil and capacitor and between the primary and secondary sides, and the magnetic field that was distributed before the power transmission was carried out.

5. Discussion on the influence of each parameter on the magnetic field strength.

It was confirmed that the calculated values using the theoretical

Table 2 Results of minimum magnetic field strength for each analysis condition.

	Size [mm]	V_1 [V]	p [mm]	N_1 [-]	η [-]	H [dBμA/m]
5.1 Fig 18(a)	1700	600	**25.1**	**11**	98.5	84.9
5.1 Fig 18(b)	1700	1100	**14.1**	**20**	98.7	84.8
5.1 Fig 18(c)	1700	1600	**9.1**	**31**	98.8	84.7
5.1 Fig 18(d)	1700	2000	**7.1**	**40**	98.9	84.7
5.2 Fig 20	**800**	600	9.1	**12**	99.0	82.0
5 -	**800**	**1400**	**6.1**	**46**	99.3	81.6

Parameters in bold are the degrees of design freedom.

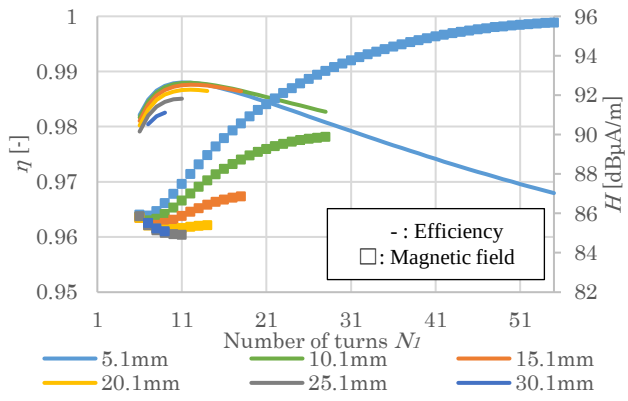

(a)600V

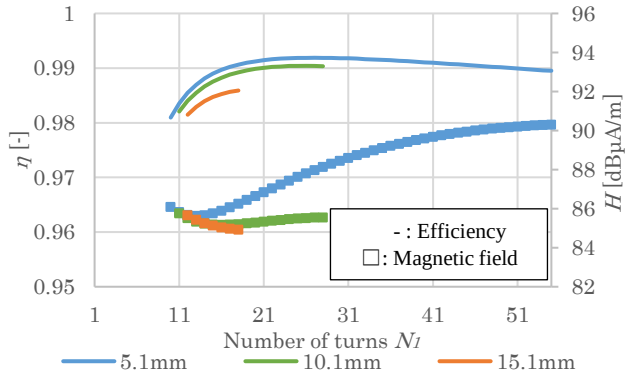

(b)1100V

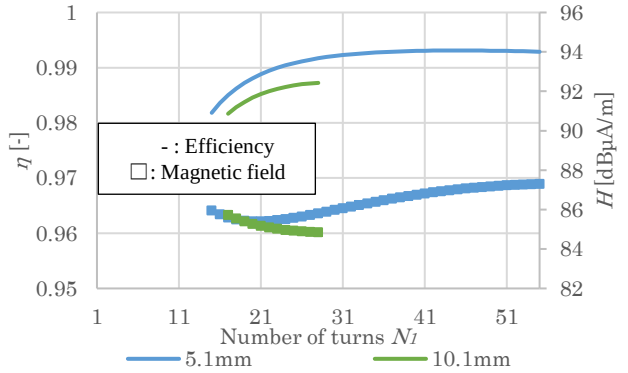

(c)1600V

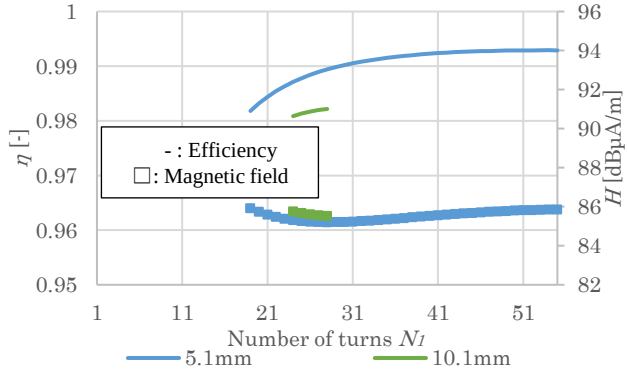

(d)2000V

Fig 18 Relationship between efficiency and magnetic field strength for the number of turns of coils on the transmission side at each pitch for each input voltage, when the transmission power is fixed at 20 kW. (-: efficiency, □: magnetic field strength)

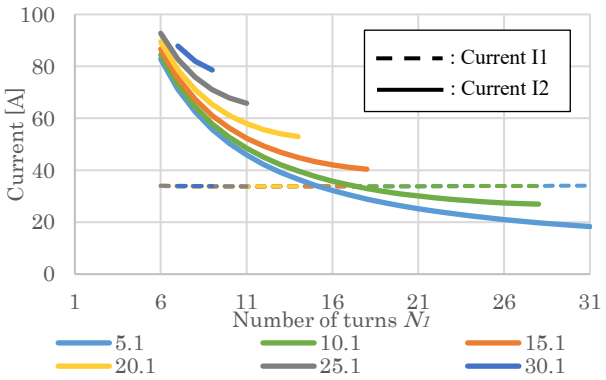

Fig 19 Relationship between primary and secondary currents at 600 V input with respect to the number of turns at each pitch.

equation derived in Chapter 4 and the measured values are in good agreement. In this section, in addition to the size, pitch, and the number of turns of the coil, the input voltage is also added as a degree of freedom in the design, and the effect of each parameter on the magnetic field strength is discussed under the conditions of 20 kW power transmission. As most of the fundamental waves of the near magnetic field strength in Chapter 4 are below 27 μT, and it is relatively easy to design below the regulation value by installation on the vehicle body and shielding, the far magnetic field strength is discussed in this section.

5.1 Behavior of number of turns, pitch and input voltage

Here, the size of the transmission coil was fixed at 1700 × 600 mm, the number of turns was changed at each pitch and the efficiency and magnetic field strength were evaluated. Similarly, this was evaluated at various input voltages.

In 5.1, coil size was fixed and the behavior of pitch and number of turns for each input voltage was confirmed. In 5.2, pitch and input voltage were fixed and graphs were presented for the behavior of coil size and number of turns. In 5.3, a summary of chapter 5 was presented. Table 2 summarizes the minimum magnetic field strength for each design condition. The parameters in bold are the parameters with design degrees of freedom.

Fig 18 shows the relationship between power transmission efficiency and magnetic field strength with regard to the number of turns at each pitch when the input voltage is set to 600 V, 1100 V, 1600 V and 2000 V respectively. Fig 18 (a) shows that at each pitch there is a number of turns for which the magnetic field strength is minimum. The magnetic field strength depends on the multiplication of the current value, coil size and the number of turns from (26) and (27). In Fig 18 the coil size is not varied, so here the current value and number of turns mainly determine the magnetic field strength. Fig 19 shows the relationship between the primary and secondary currents at each pitch in relation to the number of turns at the time of Fig 18 (a). The transmission power has been unified at 20 kW this time and the power transmission efficiency has not changed significantly, indicating that the change in the primary side current is not so large. On the other hand, the secondary-side current changes significantly in relation to the number of turns of the primary-side coil. For the secondary coil, the number of turns does not change in response to an increase in the number of turns of the primary coil, while the current value of the primary coil does not change in response to an increase in the number of turns, but the product of current value and number of turns increases in a linear shape. These changes are considered to be the reason for the existence of the number of turns and pitch at which the magnetic field strength is minimized in Fig 18. At 600 V input, with a pitch of 25.1 mm and 11 turns, the minimum value of the magnetic field strength was 84.9 dBμA/m with a power transmission efficiency of 98.5%. When the input voltage limit was lifted, at an input voltage of 2000 V, the minimum value of the magnetic field strength was 84.7 dBμA/m with a pitch of 7.1 mm and 40 turns, resulting in a power transmission efficiency of 98.9%. It can be seen that the magnetic field strength in Fig 18 (c) is more suppressed than in Fig 18 (d), but it should be noted that for reasons of clarity, the number of pitches is limited in the graph.

Unlimited the input voltage resulted in the lowest magnetic field strength at 2000V, which is the maximum in the range of parameter changes. Increasing the input voltage reduces the current when dealing with the same power and contributes to the reduction of the magnetic field strength. Table 2 shows that the reduction in magnetic field strength at 2000 V is not as great as at 1600 V input. The effect of the voltage increase is expected to increase if the power transmission is not fixed at 20 kW but unified at a higher power.

5.2 Effect of coil size on magnetic field strength

Next, the length of the transmission coil is examined. Fig 20 shows the relationship between power transmission efficiency and magnetic field strength for each coil size in relation to the number of turns when the input voltage is 600 V and the pitch is fixed at 9.1 mm. From this, it can be seen that the magnetic field strength can be reduced when the coil size is reduced. From (26) and (27), it is clear that the magnetic field strength depends on the multiplication of the current value, coil size and the number of turns, which can be correctly expressed as follows. When the input voltage and the pitch were changed simultaneously, the far magnetic field strength could be reduced to 81.6 dBμA/m when the coil size was 800 × 600 mm, the number of turns was 46 and the pitch was 6.1 mm at 1400 V input. In [30], it is shown that the coil length is economically superior as it significantly reduces the number of coils installed in the Electric Road. However, the present results show that increasing the coil size increases the magnetic field strength. It is important to select the appropriate coil in consideration of economy and safety.

5.3 Summary of the effect of coil design parameters on magnetic field strength

In 5.1, when the coil size was fixed at 1700 ×600 mm, parameters other than the coil size were changed, but the magnetic field strength did not fall below the regulated value.

In 5.2, coil size and number of turns were selected as design parameters. It was found that there was a number of turns below the regulated value of magnetic field strength for coils with a small coil size. The table shows the results when the input voltage, which is the boundary between low voltage and high voltage, is set to 600 V, when the pitch is fixed, the configuration with the minimum magnetic field strength, and when all the parameters are set to the design freedom. In this case, the coil size was 800 × 600 mm

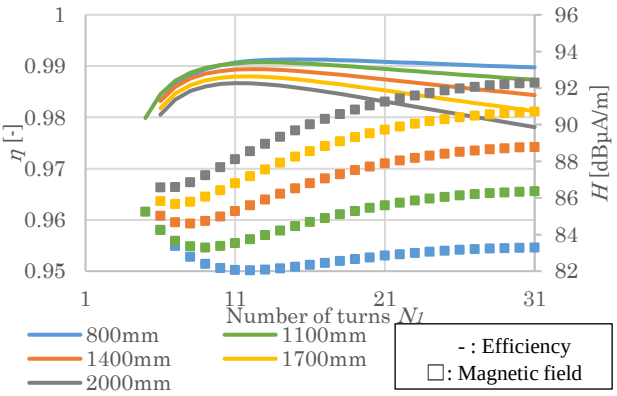

Fig 20 Relationship between efficiency and magnetic field strength for the number of turns of the coil on the transmission side for each coil size when the transmission power is fixed at 20 kW and the pitch is 9.1 mm. (-: efficiency, □: magnetic field strength)

because the variation range of the coil size was limited to the length of the receiving coil, but further reduction can be expected.

6. Conclusion

In this study, the coil design focused on the magnetic field strength as one of the key factors to ensure the safety of the coil, which is essential for the practical application of dynamic wireless power transfer to electric vehicles. In contrast to the conventional coil design using electromagnetic field analysis, which is the mainstream method, the design can be carried out using only numerical analysis, which enables fast analysis of multiple parameters, and the effect of misalignment, which frequently occurs in the case of DWPT, can be easily analyzed. The analytical results and the experimental results at low power agreed very well, showing the validity of the theory. The magnetic field strength is discussed for the far field at 11.9 m from the center of the coil and the near field at 1.1 m from the center of the coil. Both are considered at a point 1 m in the z-direction. By using this design method, the transmission distance of the main coil, misalignment, circuit configuration and load conditions can also be freely designed, and economic feasibility can be studied.

Under the condition of 20kW power transmission, the behavior of each parameter to the magnetic field strength was confirmed in simulation. When the input voltage was 600 V and the coil length was 1700 mm, the minimum value of the far magnetic field strength was 84.9 dBμA/m and the power transmission efficiency was 98.5% when the pitch was 25.1 mm and the number of turns was 11. On the other hand, when the input voltage limit was lifted, the magnetic field strength was 84.7 dBμA/m and the power transmission efficiency was 98.9% at a pitch of 7.1 mm and 40 turns at 2000 V. Increasing the input voltage could suppress the magnetic field strength and improve the efficiency. Furthermore, although not shown in the paper, taking a higher voltage has significant advantages in terms of rapid charging and downsizing of the device when considering power charging to EVs. However, the fact that a rise in input voltage is not expected to result in a very large reduction in magnetic field strength, and from the viewpoint of safety issues and infrastructure development, it is necessary to make an appropriate choice in the future.

In terms of coil size, at 600 V input, when the coil size was 800 × 600 mm with 14 turns and 10.1 mm pitch, the analyzed value showed a minimum magnetic field strength of 82.0 dBμA/m and a power transmission efficiency of 99.1%. Furthermore, when the input voltage was changed, the power transmission efficiency was 99.3% at 1400V input with a pitch of 6.1mm and 46 turns, and the magnetic field strength was 81.6 dBμA/m, the lowest value. It was shown that the coil size significantly affects the magnetic field strength. It was found that, depending on the choice of parameters, even a core-less coil can be used to lower the regulated value of 82.8 dBμA/m for the far magnetic field strength. When transmission power at 85 kHz as a regulated value of magnetic field leakage, the regulation is established not only for the magnetic field of the 85 kHz fundamental wave but also for the harmonics. Since this study only examined the fundamental wave, it remains one of the themes for future research. In addition, a coil design method based on numerical analysis during the installation of shielding material is an issue to be addressed.

References

[1] D. Patil, M. K. McDonough, J. M. Miller, B. Fahimi and P. T. Balsara, "Wireless power transfer for vehicular applications: Overview and challenges", IEEE Transactions on Transportation Electrification, vol. 4, no. 1, pp. 3-37, 2018.” .

[2] M. Yilmaz and P. T. Krein, "Review of Battery Charger Topologies, Charging Power Levels, and Infrastructure for Plug-In Electric and Hybrid Vehicles," in IEEE Transactions on Power Electronics, vol. 28, no. 5, pp. 2151-2169, May 2013, doi: 10.1109/TPEL.20.

[3] S. Li and C. C. Mi, "Wireless Power Transfer for Electric Vehicle Applications," in IEEE Journal of Emerging and Selected Topics in Power Electronics, vol. 3, no. 1, pp. 4-17, March 2015.

[4] K. W. Klontz, D. M. Divan, D. W. Novotny and R. D. Lorenz, "Contactless battery charging system," US Patent 5157319, 1991.

[5] Mariz B. Arias, Sungwoo Bae, “Electric vehicle charging demand forecasting model based on big data technologies,” Applied Energy, Volume 183, Pages 327-339, 2016.

[6] M. M. Thackeray, C. Wolvertonb and E. D. Isaacs, “Electrical energy storage for transportation－approaching the limits of, and going beyond, lithium-ion batteries,” Energy Environ. Sci., 2012, vol. 5 , 7854 -7863.

[7] S. W. Kim, D. H. Seo,X. Ma, G. Ceder and K. Kang, “Electrode Materials for Rechargeable Sodium-Ion Batteries: Potential Alternatives to Current Lithium-Ion Batteries,” ADVANCED ENERGY MATERIALS, Vol. 2, Issure 7, July, 2012.

[8] S. Jeong, Y. J. Jang, D. Kum and M. S. Lee, "Charging Automation for Electric Vehicles: Is a Smaller Battery Good for the Wireless Charging Electric Vehicles?," in IEEE Transactions on Automation Science and Engineering, vol. 16, no. 1, pp. 486-497, Jan.

[9] S. Jeong, Y. J. Jang and D. Kum, "Economic Analysis of the Dynamic Charging Electric Vehicle," in IEEE Transactions on Power Electronics, vol. 30, no. 11, pp. 6368-6377, Nov. 2015, doi: 10.1109/TPEL.2015.2424712.

[10] A. Arora, N. Niese, E. Dreyer, A. Waas and A. Xie, "Why Electric Cars Can't Come Fast Enough," 2021 April published, 2022 November viewed, BCG, https://www.bcg.com/ja-jp/publications/2021/why-evs-need-to-accelerate-their-market-penetration.

[11] A. Mahesh, B. Chokkalingam and L. Mihet-Popa, "Inductive Wireless Power Transfer Charging for Electric Vehicles－A Review," in IEEE Access, vol. 9, pp. 137667-137713, 2021, doi: 10.1109/ACCESS.2021.3116678..

[12] P. D. Aghcheghloo, D. J. Wilson and T. Larkin, "Towards the Electrification of Road Infrastructure," Equity in Transportation, New Zealand, Mar. 2020.

[13] Wen, F.; Huang, X. "Optimal Magnetic Field Shielding Method by Metallic Sheets in Wireless Power Transfer System," Energies 2016, 9, 733. https://doi.org/10.3390/en9090733.

[14] M. Curti, J. J. H. Paulides and E. A. Lomonova, "An overview of analytical methods for magnetic field computation," 2015 Tenth International Conference on Ecological Vehicles and Renewable Energies (EVER), 2015, pp. 1-7, doi: 10.1109/EVER.2015.7112938.

[15] B. J. Limb et al., "Economic Viability and Environmental Impact of In-Motion Wireless Power Transfer," in IEEE Transactions on Transportation Electrification, vol. 5, no. 1, pp. 135-146, March 2019.

[16] A. Shekhar, M. Bolech, V. Prasanth and P. Bauer, "Economic considerations for on-road wireless charging systems - A case study," 2015 IEEE PELS Workshop on Emerging Technologies: Wireless Power (2015 WoW), 2015, pp. 1-5, doi: 10.1109/WoW.2015.7132804.

[17] Wen, F.; Huang, X. Human Exposure to Electromagnetic Fields from Parallel Wireless Power Transfer Systems. Int. J. Environ. Res. Public Health 2017, 14, 157. https://doi.org/10.3390/ijerph14020157.

[18] SAE International, "Wireless Power Transfer for Light-Duty Plug-in/Electric Vehicles and Alignment Methodology J2954," Issued2016-05, Revised2020-10.

[19] International commission on Non-Ionizing Radiation Protection, "Guidelines for limiting exposure to time-varying electric, magnetic, and electromagnetic fields(up to 300GHz)(1Hz To 100kHz)," Health Phys. 2010, 99, 818-836.

[20] IEC International Electrotechinical Commission, "CiSPR 11 Consolidated version," Jan 18, 2019 Publicated.

[21] B. Zhang et al., "Concept Design of Active Shielding for Dynamic Wireless Charging of Light-duty EV," 2020 IEEE Transportation Electrification Conference & Expo (ITEC), 2020, pp. 844-850, doi: 10.1109/ITEC48692.2020.9161606.

[22] T. Campi, S. Cruciani, F. Maradei and M. Feliziani, "Active Coil System for Magnetic Field Reduction in an Automotive Wireless Power Transfer System," 2019 IEEE International Symposium on Electromagnetic Compatibility, Signal & Power Integrity (EMC+SIPI),.

[23] S. Y. Choi, B. W. Gu, S. W. Lee, W. Y. Lee, J. Huh and C. T. Rim, "Generalized Active EMF Cancel Methods for Wireless Electric Vehicles," in IEEE Transactions on Power Electronics, vol. 29, no. 11, pp. 5770-5783, Nov. 2014, doi: 10.1109/TPEL.2013.2295094.

[24] Y. Yamada, S. Hasegawa, T. Imura and Y. Hori, "Design Method of Coreless Coil Considering Power, Efficiency and Magnetic Field Leakage in Wireless Power Transfer," the 48th Annual Conference of the IEEE Industrial Electronics Society (IES), IECON2022, Bru.

[25] T. Imura, "Wireless Power Transfer : Using Magnetic and Electric Resonance Coupling Techniques," Springer, 2020..

[26] Y. Yamada and T. Imura, "An Efficiency Optimization Method of Static Wireless Power Transfer Coreless Coils for Electric Vehicles in the 85 kHz Band Using Numerical Analysis," IEEJ, Transactions on Electrical and Electronic Engineering, Vol.17No.10, 2022.

[27] Richard Y. Zhang, Jacob K. White, and John G. Kassakian, Charles R.Sullivan, "Realistic Litz Wire Characterization using Fast Numerical Simulations", in Applied Power Electoronics Conference and Exposition, pp.738-745, 2014.".

[28] S. S. Mohan, M. del Mar Hershenson, S. P. Boyd and T. H. Lee, "Simple accurate expressions for planar spiral inductances," in IEEE Journal of Solid-State Circuits, vol. 34, no. 10, pp. 1419-1424, Oct. 1999, doi: 10.1109/4.792620..

[29] H. Ikoma, S. Kogoshi and Y. Murata, "Koukano Dennzikigaku" Baihuukann, 2000, in Japanese..

[30] Y. Yamada, K. Sasaki, T. Imura and Y. Hori, "Design Method of Coils for Dynamic Wireless Power Transfer Considering Average Transmission Power and Installation Rate," IEEE 6th Southern Power Electronics Conference (SPEC 2021), Kigali Rwanda.

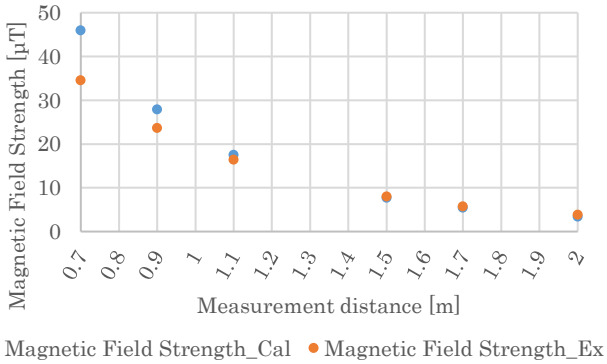

Fig A1 Relation between measurement point and error of near magnetic field strength.

Appendix

1) Accuracy of the derivation of the near magnetic field strength

In this study, vector potentials were used to derive the magnetic field strength. The vector potential is derived using the approximation that the distance from the coil to the measurement point is sufficiently large for the size of the coil. However, the measurement points of the near magnetic field strength in this study are 1.1 m in the y-direction and 1 m in the z-direction from the center of the coil, which is not far away since the coil size is 1700 x 600 mm. Therefore, the distance of the measurement points and the accuracy of the derivation are summarized in Fig A1. It can be seen that the closer the measurement point is to the coil, the further apart the measured and theoretical values are. The error rate at 0.7 m in the y-direction and 1 m in the z direction was -24.7%. The error rate at 1.1 m from the y-direction and 1 m in the z-direction was -6.0%, while at a distance of 1.5 m from the y-direction, the error rate decreased to 3.9%. However, when the measurement point is further away, the error rate tends to increase, although it is not noticeable on the graph. This may be since the magnetic field strength is reduced, making it more susceptible to magnetic fields other than those from the coil. The regulated value of the near magnetic field is 27 μT, and since it was 16 μT this time during 20 kW power transmission, there is no problem even if the error rate is 6%. However, in the case of power transmission at even higher power levels, it is necessary to analyze the near magnetic leakage field in detail by an electromagnetic field analysis, but in reality, the power receiving coil is attached to the car body, and the near magnetic field leakage can be greatly suppressed by the car body and shielding material. Therefore, it is important to take adequate countermeasures against far magnetic field leakage.

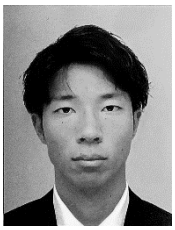

Yuto Yamada (Student Member) He entered the Department of Electrical Engineering, Faculty of Science and Technology, Tokyo University of Science in April 2017, graduated in March 2021, and entered the Department of Electrical Engineering, Graduate School of Science and Technology, Tokyo University of Science in April 2021. He is currently focusing on the design of coils and circuit for wireless power transfer to electric vehicles and the realization of Dynamic Wireless Power Transfer. He is a student member of the Institute of Electrical and Electronics Engineers (IEEE) and the Institute of Electrical Engineers of Japan (IEEJ).

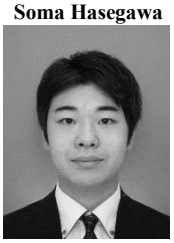

Soma Hasegawa (Student Member) He entered the Department of Electrical Engineering, Faculty of Science and Technology, Tokyo University of Science in April 2017, graduated in March 2021, and entered the Department of Electrical Engineering, Graduate School of Science and Technology, Tokyo University of Science in April 2021. He is currently focusing on the Magnetic field leakage from Wireless Power Transfer Coils to electric vehicles and the realization of Dynamic Wireless Power Transfer. He is a student member of the Institute of Electrical Engineers of Japan (IEEJ).

Takehiro Imura (Member) Received the bachelor's degree in electrical and electronics engineering from Sophia University, Tokyo, Japan, in 2005, and the M.E. degree in electronic engineering and the D.Eng. degree in electrical engineering from The University of Tokyo, Tokyo, in 2007 and 2010, respectively. He joined the Department of Advanced Energy, Graduate School of Frontier Sciences, University of Tokyo, as a Research Associate, where since 2015, he has been a Project Lecturer. In 2019, he joined the Department of Electrical Engineering, Tokyo University of Science, as an Associate Professor. He is currently investigating wireless power transfer using magnetic resonant coupling and electric resonant coupling. His research interests include electric vehicle in-motion connected to renewable energy, sensors and cancer treatment. He is the winner of the IEEJ Industry Applications Society Distinguished Transaction Paper Award in 2015, of the IEEE Power Electronics Transactions First Prize Paper Award in 2017. He is a member of the Institute of Electrical and Electronics Engineers (IEEE), the Institute of Electronics, Information and Communication Engineers (IEICE), and the Society of Automotive Engineers of Japan (JSAE).

Yoichi Hori (Fellow) Yoichi Hori received his B.S., M.S., and Ph.D. degrees in Electrical Engineering from the University of Tokyo, Tokyo, Japan, in 1978, 1980, and 1983, respectively. In 1983, he joined the Department of Electrical Engineering, The University of Tokyo, as a Research Associate. He later became an Assistant Professor, an Associate Professor, and, in 2000, a Professor at the same university. In 2002, he moved to the Institute of Industrial Science as a Professor in the Information and System Division, and in 2008, to the Department of Advanced Energy, Graduate School of Frontier Sciences, the University of Tokyo. He retired in March 2021, and has been in current position since April. Professor Emeritus of the University of Tokyo. From 1991-1992, he was a Visiting Researcher at the University of California at Berkeley. His research fields are control theory and its industrial applications to motion control, mechatronics, robotics, electric vehicles, etc. Recently, he has also been focusing on the research and promotion of wireless power transfer. He is a Life Fellow of IEEE (the Institute of Electrical and Electronics Engineers) and a past AdCom member of IES (Industrial Electronics Society). He has been the Treasurer of the IEEE Japan Council and Tokyo Section in a few years since 2001. He is now the Fellow members of IEEJ (the Institute of Electrical Engineers of Japan), JSAE (the Society of Automotive Engineers of Japan), JSST (Japan Society of Simulation Technology), and so on. He was the Presidents of the Industry Applications Society of the IEEJ, and WEVA (World Electric Vehicle Association), the Director of Japan Automobile Research Institute (JARI), and the Vice-President of JSAE. He is now the President of Capacitors Forum, the Chairman of Motor Technology Symposium of JMA (Japan Management Association), and the Representative Director of NeV (Next Generation Vehicle Promotion Center), and so on. He is the winner of the Best Transactions Paper Award from the IEEE Transactions on Industrial Electronics in 1993, 2001 and 2013, of the 2000 Best Transactions Paper Award from IEEJ, and 2011 Achievement Award of IEEJ.